Supporting information

Engineering highly active surfaces in molybdenum-integrated cobalt telluride electrodes for enhanced battery-type charge-storage in supercapacitors

Dhanasekaran Vikraman[a], Sajjad Hussain[b,c], K. Karuppasamy[d,e], Hyeon-Wook Yu[a], Muhammad Ali[f], Anandhavelu Sanmugam[g], Jongwan Jung[b,c], Akram Alfantazi[d,e], Hyun-Seok Kim[a*]

[a.]Division of Electronics and Electrical Engineering, Dongguk University-Seoul, Seoul 04620, Republic of Korea.

[b.]Department of Nanotechnology and Advanced Materials Engineering, Sejong University, Seoul 05006, Republic of Korea.

[c.]Hybrid Materials Center (HMC), Sejong University, Seoul 05006, Republic of Korea.

[d.]Emirates Nuclear Technology Center (ENTC), Khalifa University of Science and Technology, Abu Dhabi, 127788, United Arab Emirates.

[e.]Department of Chemical and Petroleum Engineering, Khalifa University of Science and Technology, Abu Dhabi, 127788, United Arab Emirates.

[f.]Interdisciplinary Research Center for Hydrogen Technologies and Carbon Management (IRC-HTCM), King Fahd University of Petroleum & Minerals, KFUPM Box 5040, Dhahran, 31261, Saudi Arabia.

[g.]Department of Applied Chemistry, Sri Venkateswara College of Engineering, Pennalur, Sriperumbudur 602117, India.

*Email: hyunseokk@dongguk.edu; Tel.: +82-2-2260-3996; Fax: +82-2-2277-8735

S1. Preparation of $CoTe_2$ nanostructures

Sulfuric acid-treated TeO_2 (1.5 mM) was mixed with an aqueous $(NH_4)_2Co(SO_4)_2$ solution (2 mM) under vigorous magnetic stirring at room temperature for 1 h. Subsequently, 2 mL of N_2H_4 and 4 mL of NH_4OH were slowly introduced under continuous stirring to obtain a homogeneous reaction mixture. The mixture was then heated on a hot plate at 80 °C for 3 h while maintaining constant agitation. After cooling naturally to room temperature, the resulting precipitate was collected and washed several times with DI water and ethanol via centrifugation. The black $CoTe_2$ powder was then dehydrated at 60 °C for 3 h in a hot-air oven and finally calcined in a tellurium atmosphere at 500 °C for 2 h.

S2. Preparation of $MoTe_2$ nanostructures

Sulfuric acid-treated TeO_2 (1.5 mM) was mixed with a $(NH_4)_6Mo_7O_{24}$ solution (2 mM) under vigorous magnetic stirring at room temperature for 1 h. Afterwards, 2 mL of N_2H_4 and 2 mL of NH_4OH were slowly added under continuous magnetic stirring to form a uniform solution mixture. The reaction mixture was then heated at 80 °C for 3 h with constant stirring. After gradually cooling to room temperature, the resulting precipitate was collected and rinsed with DI water and ethanol by centrifugation. The black $MoTe_2$ powder was dehydrated at 60 °C for 3 h and then calcined in a tellurium environment at 500 °C for 2 h.

S3. Characterisations

The physical properties of the synthesized Co_xTe_2-based nanostructures were analysed using the following instruments: JEOL JSM-6700F field-emission scanning electron microscope; JEOL-2010F transmission electron microscope; Microtrac BELsorp-mini II system at 77 K for BET analysis; Renishaw inVia RE04 Raman spectrometer; and PHI 5000 VersaProbe II X-ray photoelectron spectrometer.

Mass calculation:

The mass loading of AC in the asymmetric device was calculated based on equation S1.

$$\frac{m_+}{m_-} = \frac{C_{Sp-} \times \Delta V_-}{C_{Sp+} \times \Delta V_+} \quad \text{(S1)}$$

where m_- and m_+ represent the mass of active materials, C_s^- and C_s^+ represent specific capacity, ΔV_- and ΔV_+ represent the potential windows for the negative and positive electrodes, respectively.

The ASC device-specific capacitance (C_{SC}) was estimated using equation (S2)

$$C_{SC} = \frac{i\,(\Delta t)}{w(\Delta V)} \quad \text{(S2)}$$

The energy density and power density parameters of ASCs were obtained via the following relationships.

$$E = \frac{C_{SC} \times (\Delta V)^2}{2 \times 3.6} \quad \text{(S3)}$$

$$P = \frac{E}{\Delta t} \quad \text{(S4)}$$

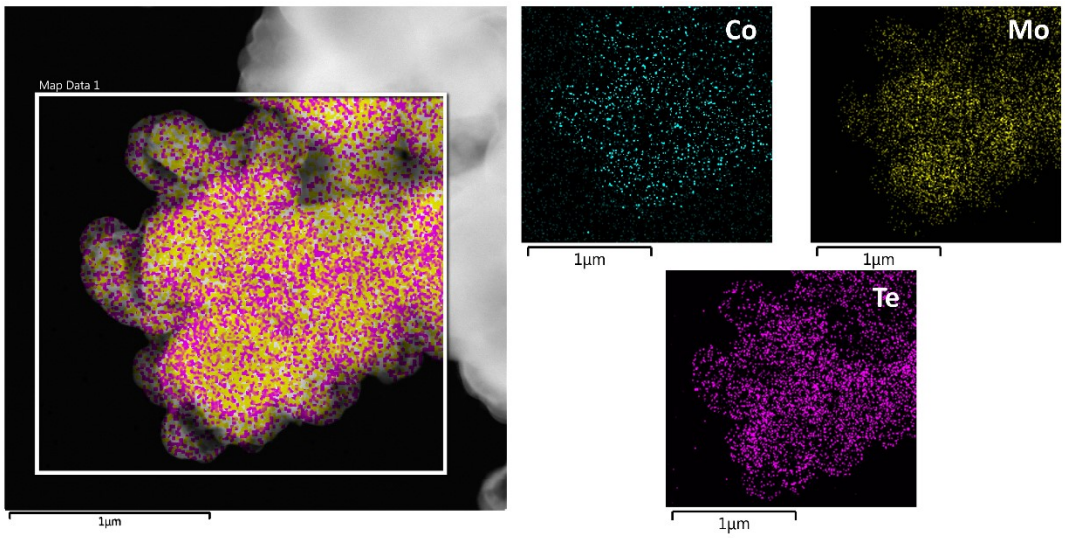

Figure S1. TEM elemental mapping of MCT-1 and corresponding distributions of Co, Mo, and Te.

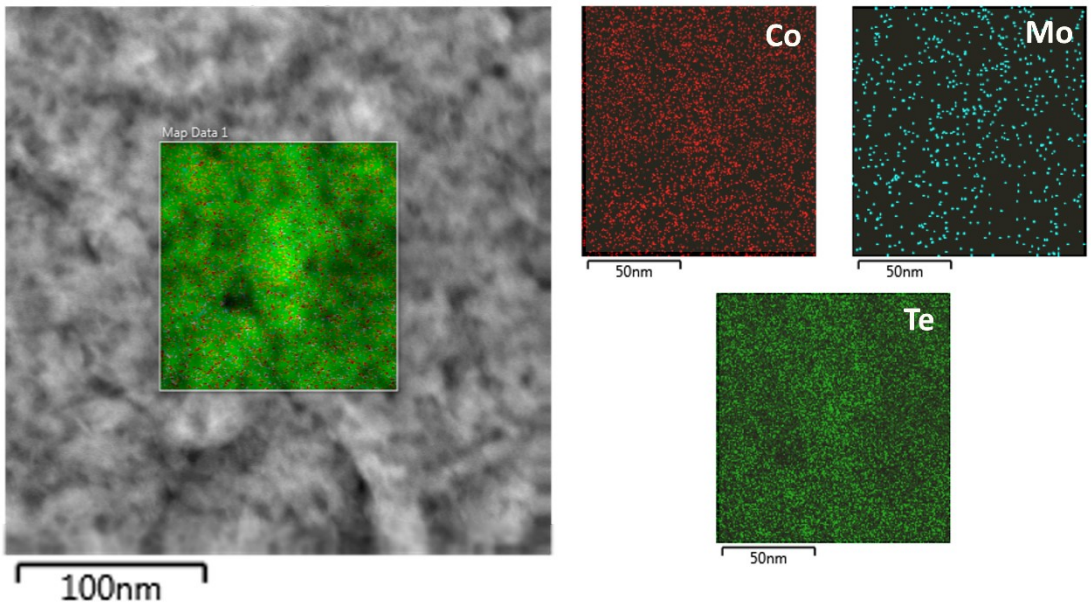

Figure S2. TEM elemental mapping of MCT-2 and corresponding distributions of Co, Mo, and Te.

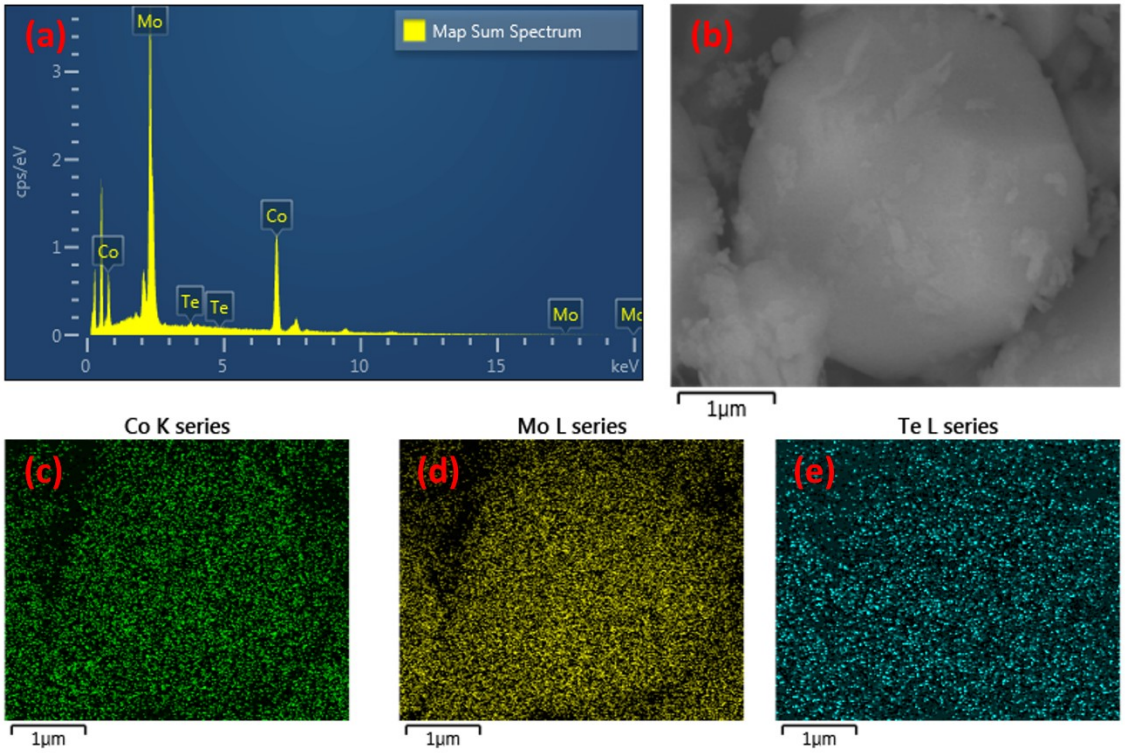

Figure S3. (a) EDS spectrum of MCT-3; elemental mapping of MCT-3 shown by (b) SEM mapping and corresponding distributions of (c) Co, (d) Mo, and (e) Te.

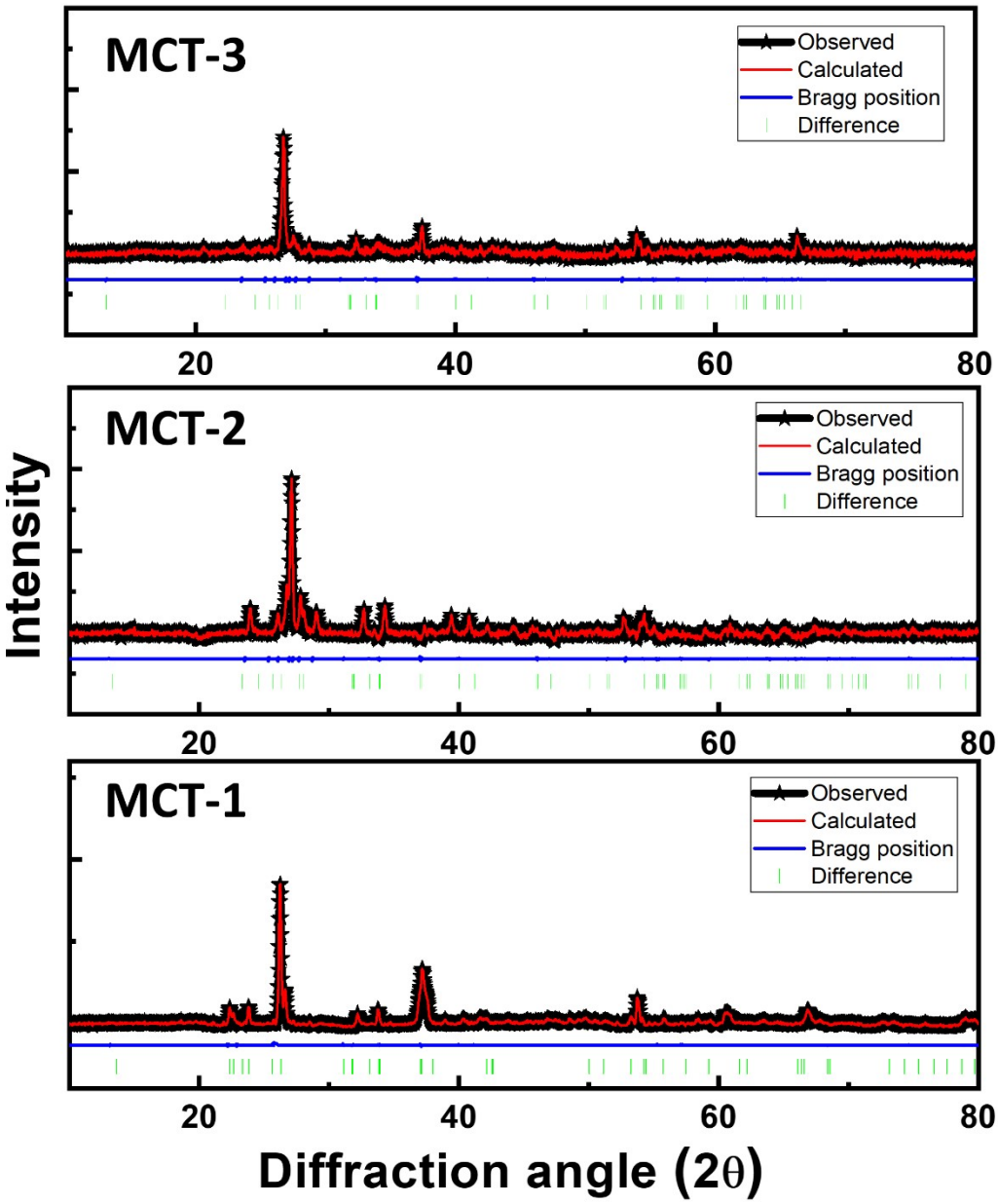

Figure S4. Rietveld refinement on MCT-1, MCT-2, and MCT-3 patterns.

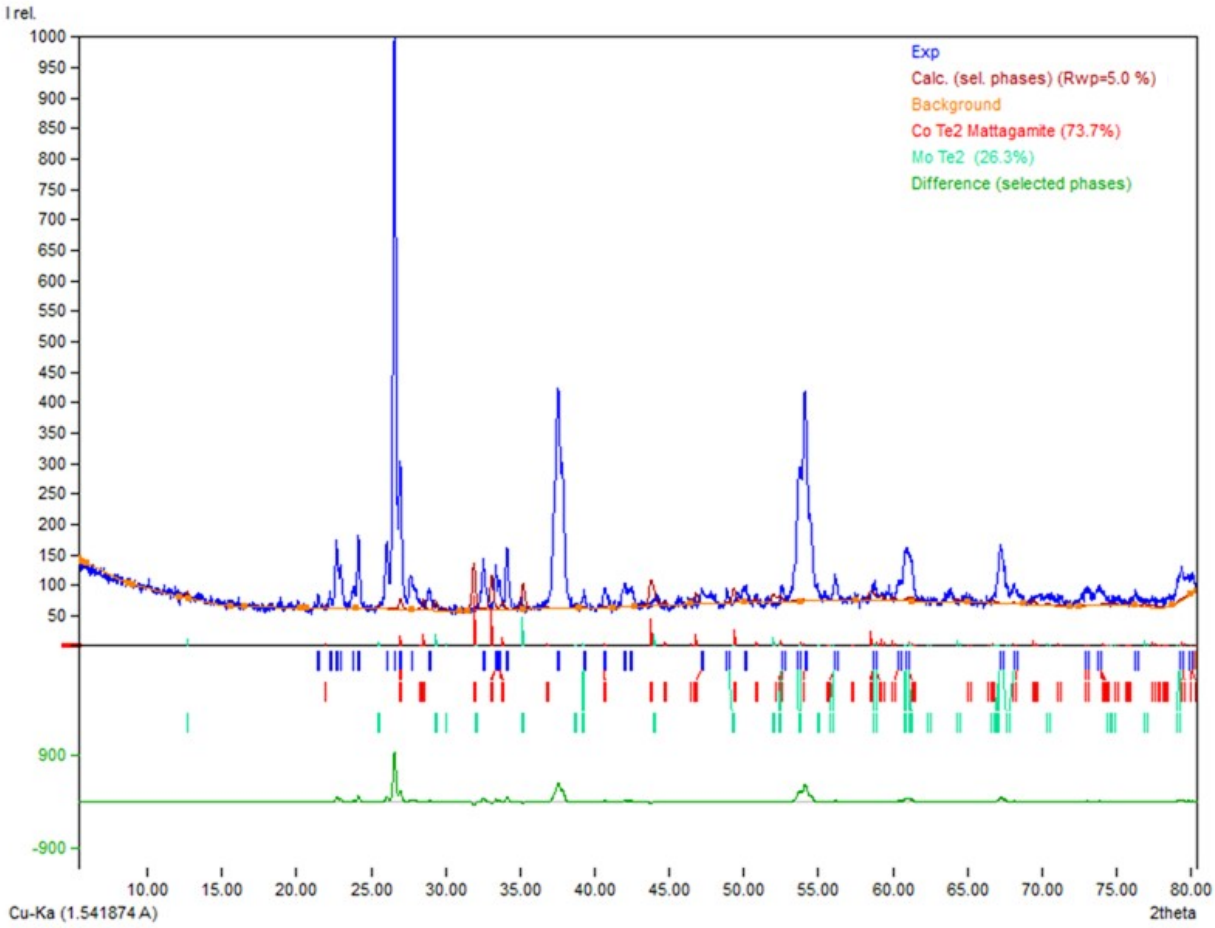

Figure S5. Phase composition ratio of MCT-1 solid solution.

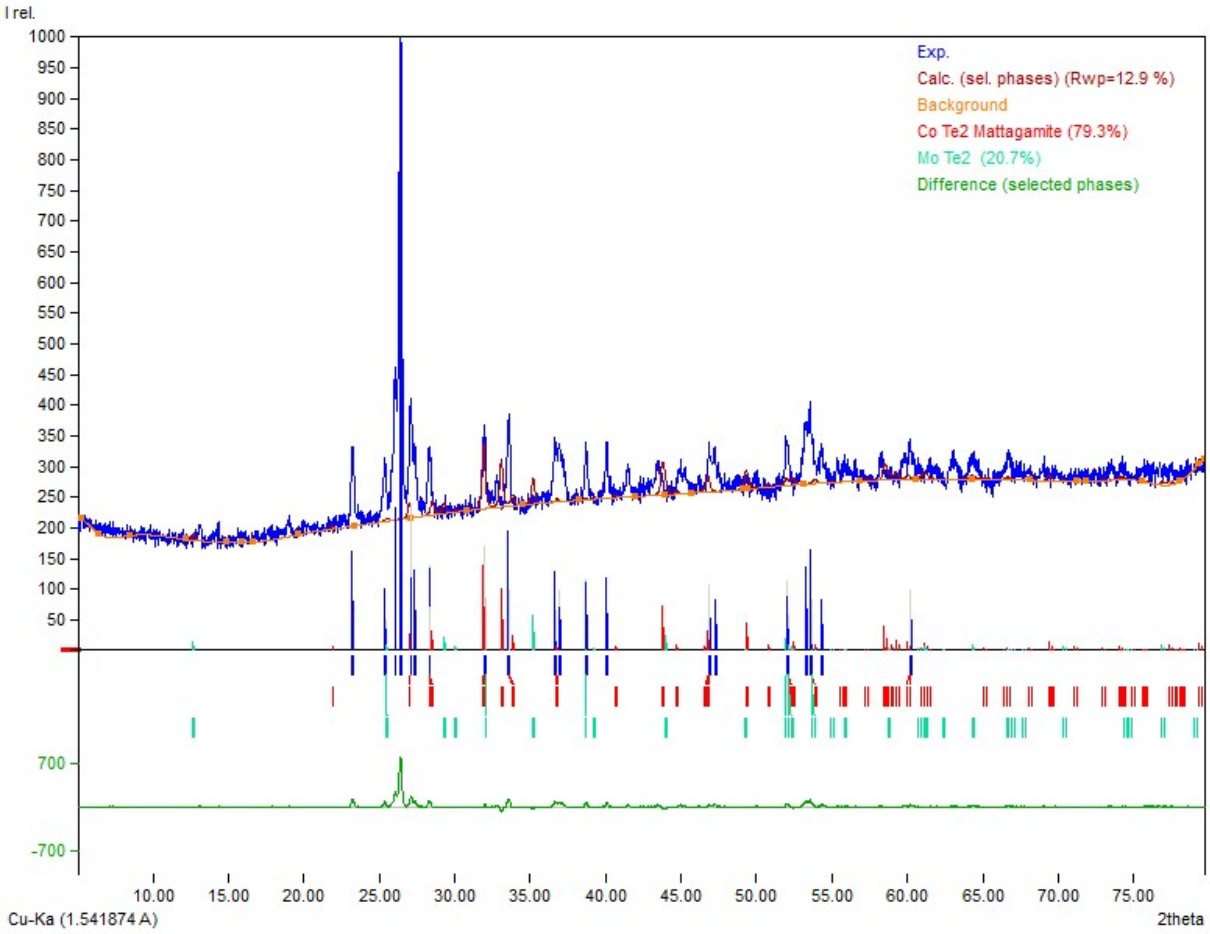

Figure S6. Phase composition ratio of MCT-2 solid solution.

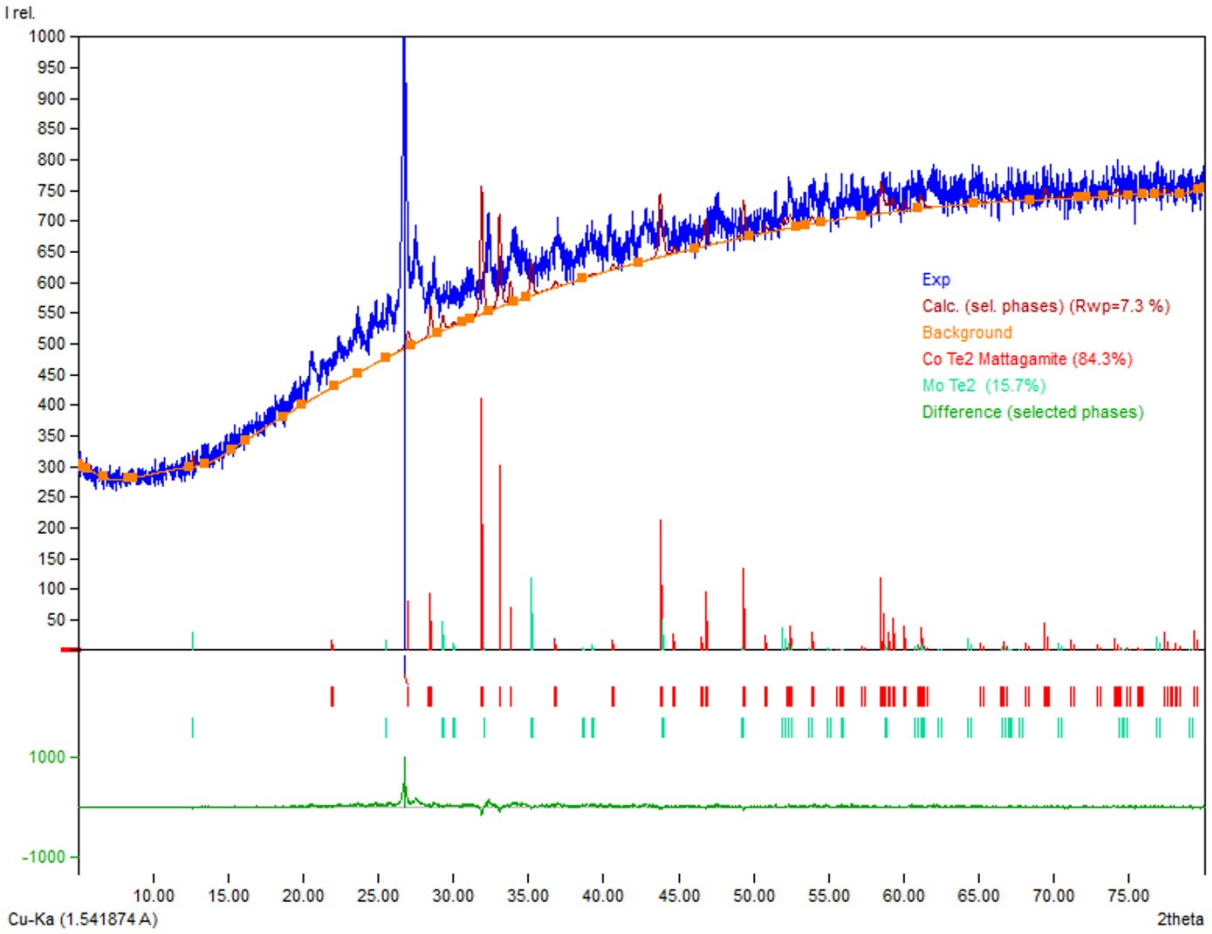

Figure S7. Phase composition ratio of MCT-3 solid solution.

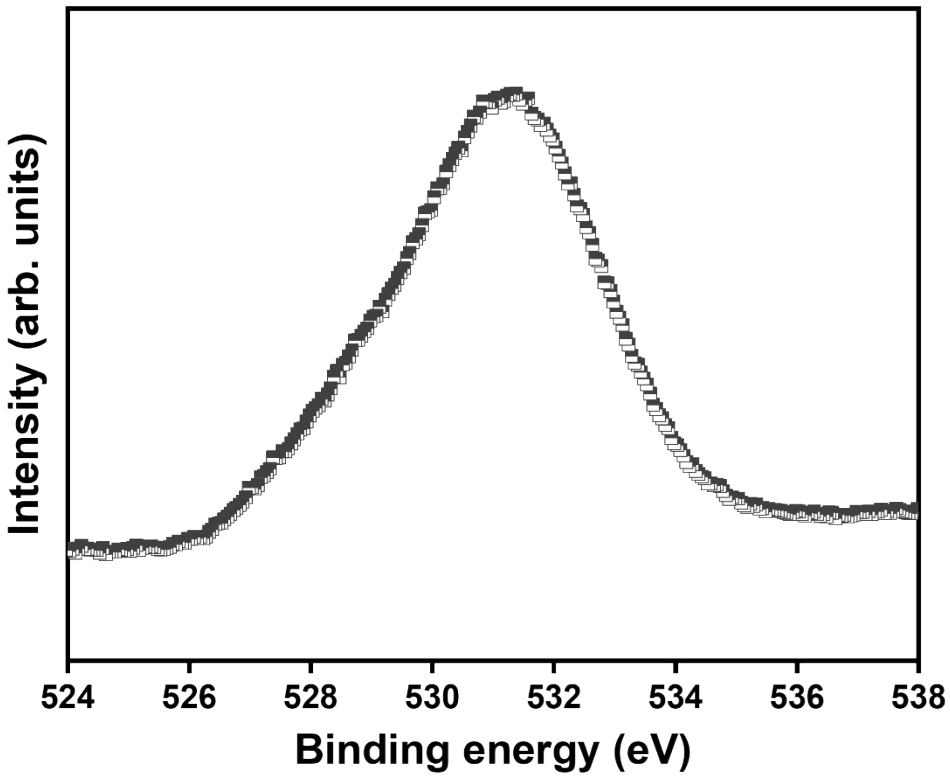

Figure S8. O 1s XPS profile for MCT-3 structure.

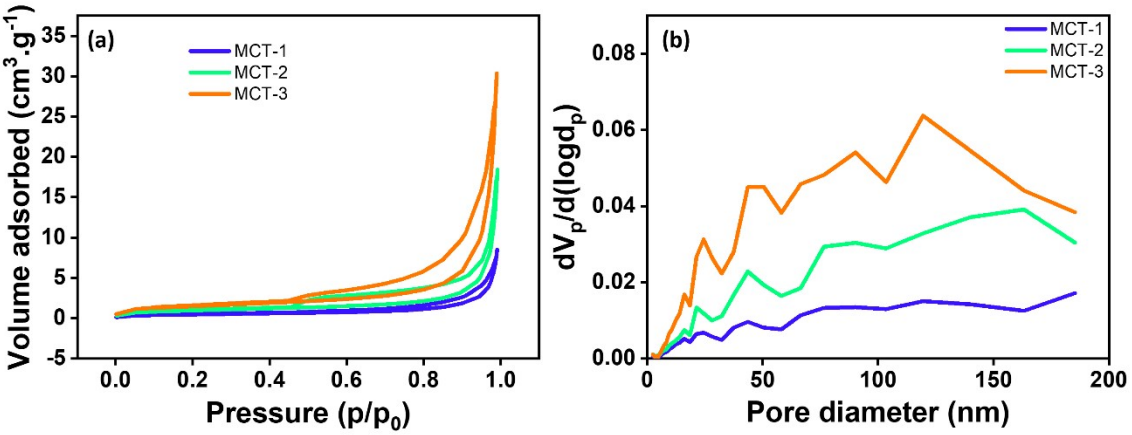

Figure S9. (a) BET surface-area profiles and (b) BJH pore-size distribution curves for MCT-1, MCT-2, and MCT-3 nanostructures.

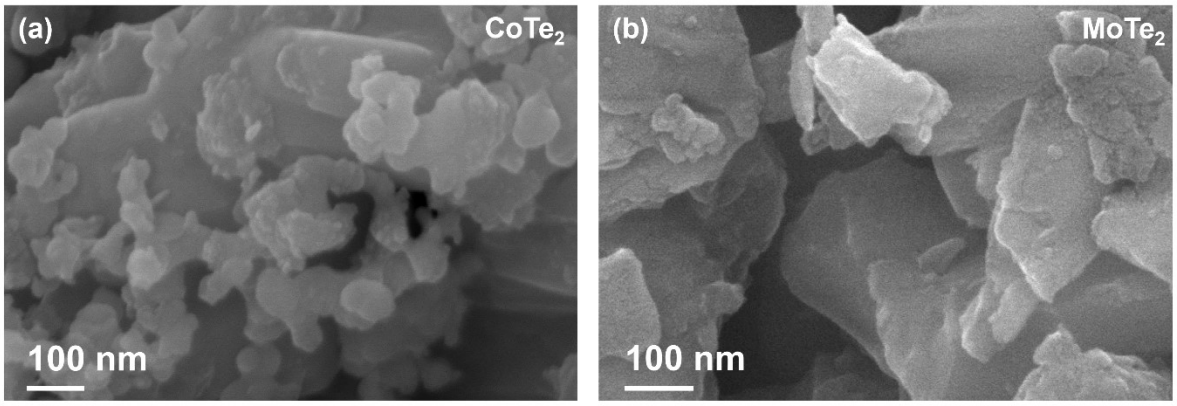

Figure S10. SEM of (a) $CoTe_2$ and (b) $MoTe_2$ nanostructures.

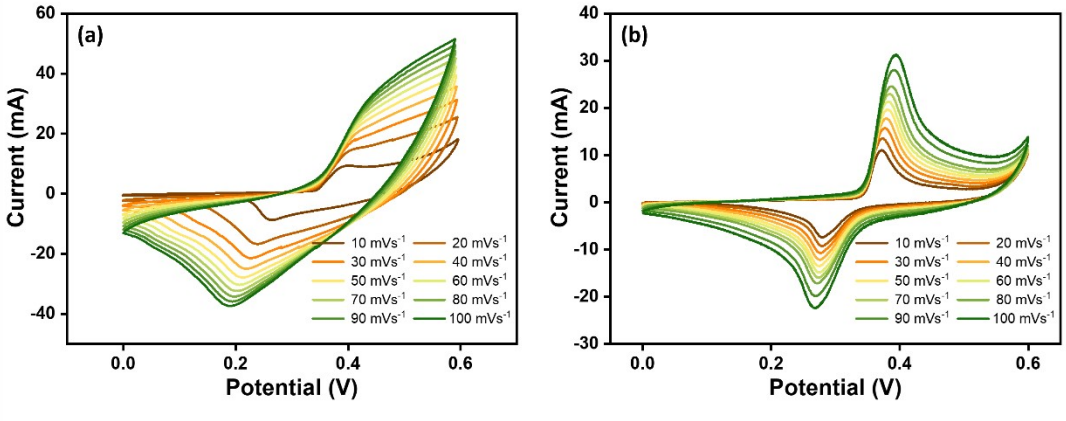

Figure S11. CV profiles of (a) $CoTe_2$ and (b) $MoTe_2$ nanostructures recorded at various scan rates.

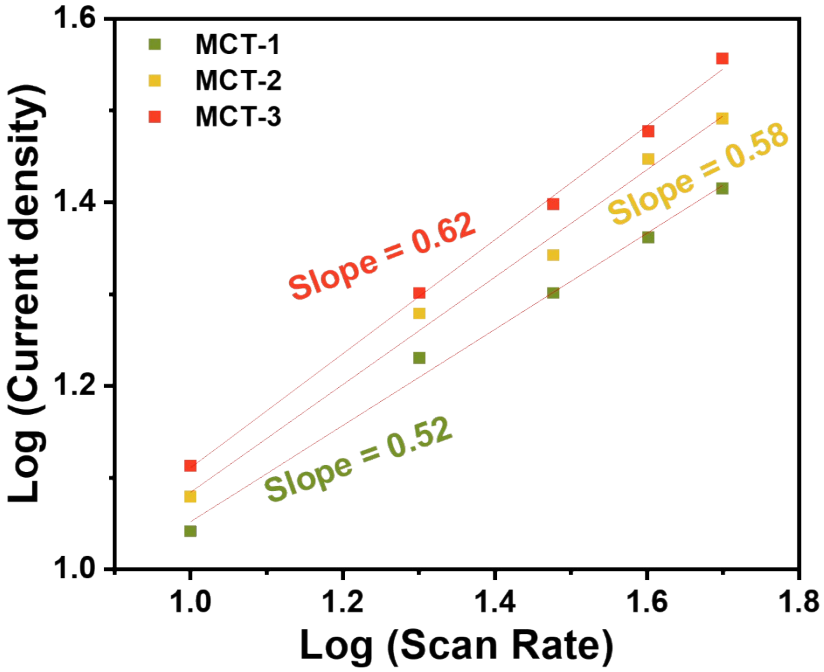

Figure S12. Plot of current density vs scan rate for MCT-1, MCT-2, and MCT-3 nanostructures.

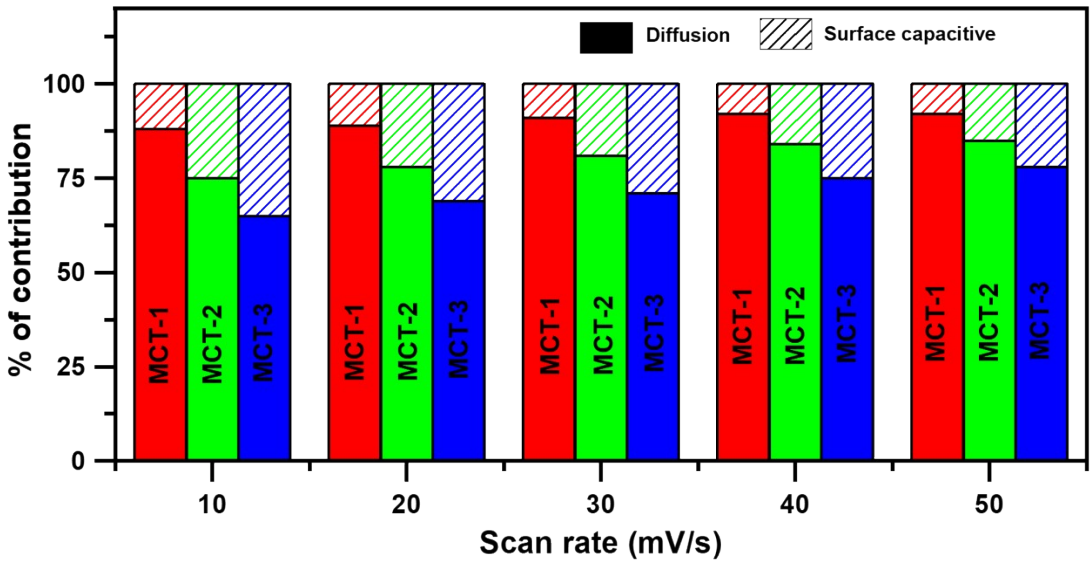

Figure S13. The capacitive and diffusive charge contribution in the MCT-1, MCT-2, and MCT-3 nanostructures electrodes as a function of the scan rate.

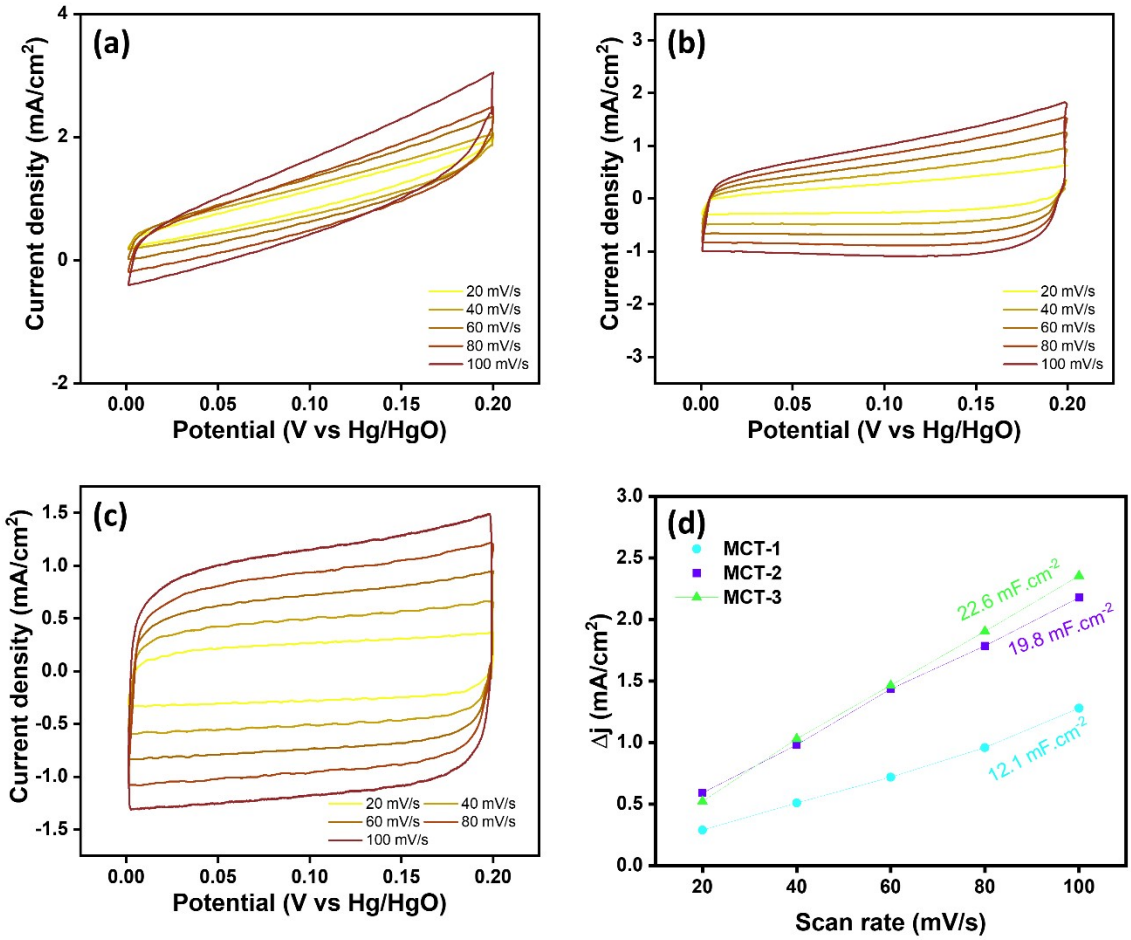

Figure S14. Non-faradaic region CVs at different scan rates for the (a) MCT-1, (b) MCT-2, and (c) MCT-3 nanostructures; current density variations at 0.1 V vs Hg/HgO for MCT-1, MCT-2, and MCT-3 nanostructures.

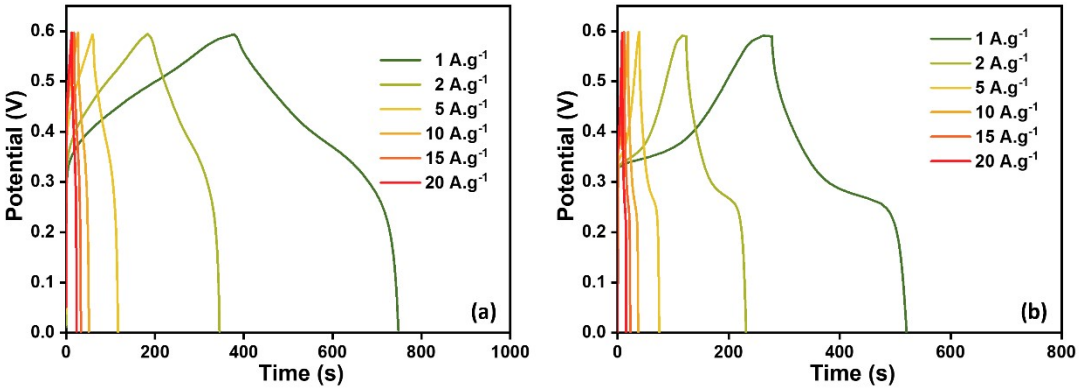

Figure S15. GCD profiles of (a) $CoTe_2$ and (b) $MoTe_2$ nanostructures at different applied current densities.

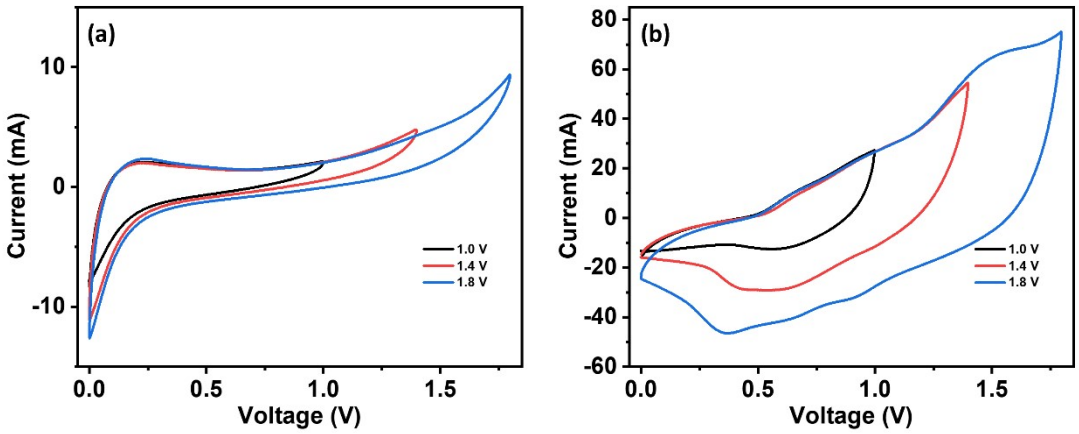

Figure S16. CV profiles of (a) MCT-1//AC and (b) MCT-2//AC asymmetric devices at different voltage windows.

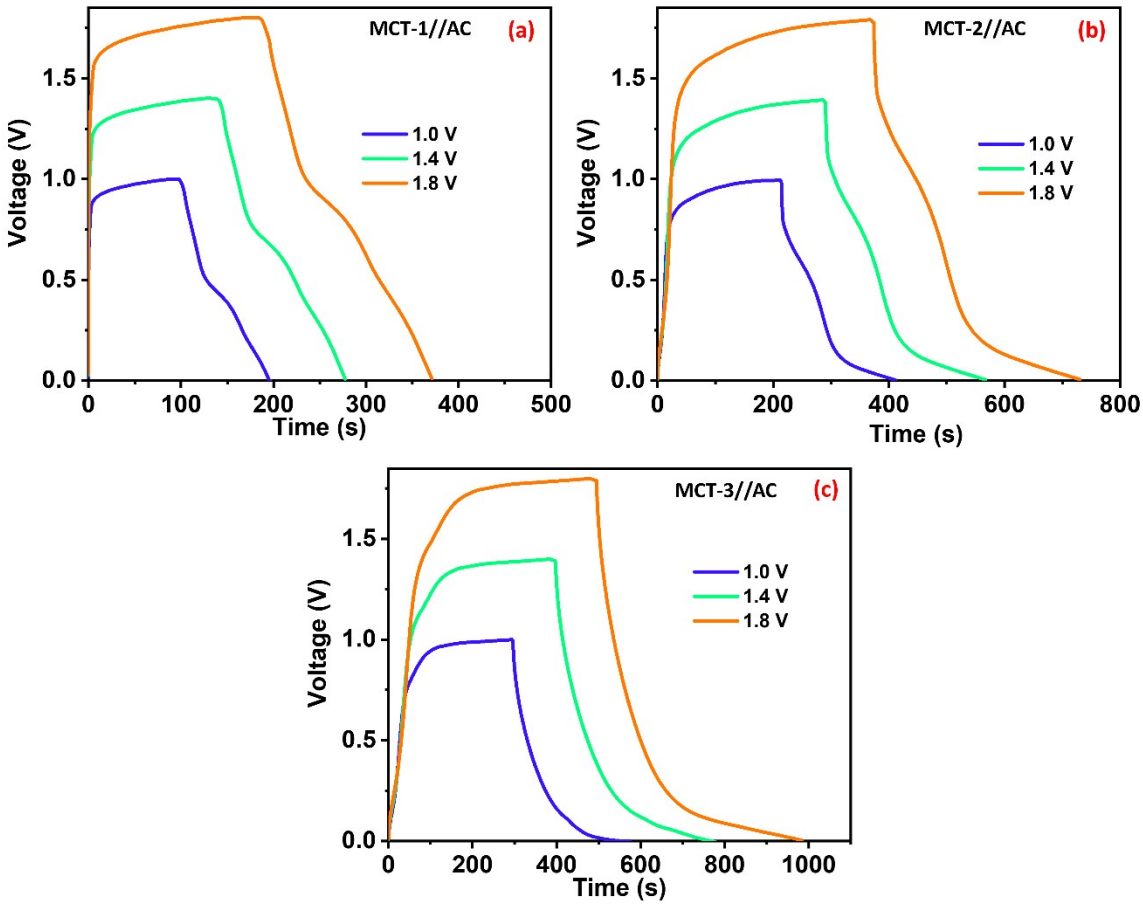

Figure S17. GCD profiles of (a) MCT-1//AC, (b) MCT-2//AC and (c) MCT-3//AC asymmetric devices at different voltage windows.

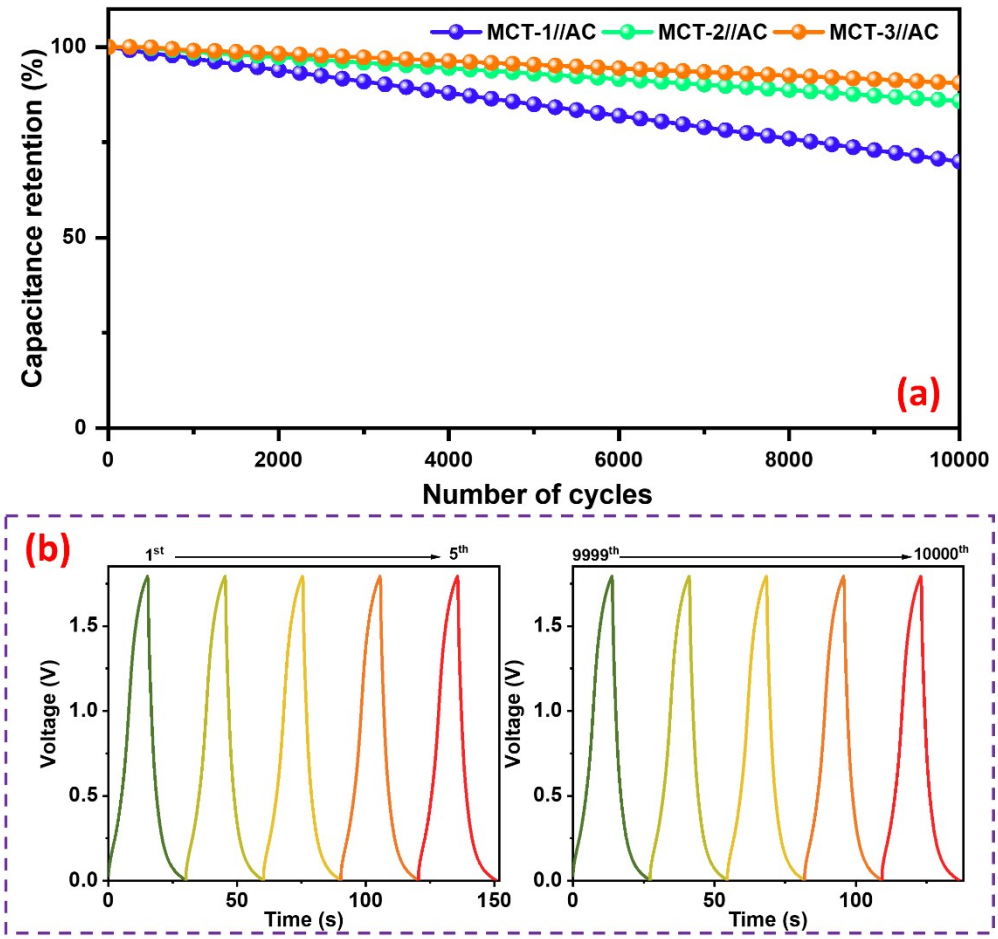

Figure S18. (a) Capacity retention of MCT-1, MCT-2 and MCT-3 at 20 A g^{-1} ; (b) initial and final five GCD cycles for MCT-3.

Table S1. N_2 sorption analysis parameters for MCT-1, MCT-2, and MCT-3 nanostructures.

Sample	BET ($m^2.g^{-1}$)	Pore volume ($cm^3.g^{-1}$)	Mean pore diameter (nm)
MCT-1	1.68	0.012	29.2
MCT-2	3.51	0.026	29.7
MCT-3	5.21	0.046	35.7

Table S2. Three-electrode supercapacitor performance comparison with TMDs electrodes.

Electrode materials	Electrolyte (M)	Specific capacitance	Capacitance retention (%)/ cycles	Ref.
MCT-3	***1 KOH***	***691 C·g^{-1} (1151 F·g^{-1}) @ 1 A·g^{-1}***	***98 / 10000***	***In this study***
CoTe	3 M KOH	622.8 F·g^{-1} @ 1 A·g^{-1}	85 / 2000	[1]
$NiTe_2$	3 M KOH	804 F g^{-1} @ 1 A g^{-1}	91.3 / 1000	[2]
NiTe/ZIF-67	3 M KOH	1521 F·g^{-1} @ 1A·g^{-1}	93.5/5000	[3]
$MoTe_2$/graphene	1 M Na_2SO_4	434 ± 37.5 F g^{-1} @1A g^{-1}	-	[4]
$MoTe_2$	1.0 M KOH	416 F·g^{-1} @ 2 A·g^{-1}	97.1% /5000	[5]
CuTe-CoTe@ $NiTe_2$	6 M KOH	1481 F·g^{-1} @ 1 A·g^{-1}	92.15 / 10000	[6]
MWCNTs/$MoTe_2$	1 M NaOH	502 F g^{-1}@ 2 mV s^{-1}	81 / 5000	[7]
CoTe/$NiCo_2S_4$	3 M KOH	1470.45 F g^{-1} @ 1 A g^{-1}	86.69 / 5000	[8]
$NiCoTe_2$	6 K KOH	2006 F·g^{-1} @ 1 A·g^{-1}	96.15 / 20000	[9]
$CoTe_2$ nanoflowers	1 M KOH	460 F g^{-1}@ 1.5 A g^{-1}	91 / 5000	[10]
$NiTe_2$-Co_2Te_2@rGO	1 M KOH	223.6 mAh g^{-1} at 1 A g^{-1}	89.3 / 3000	[11]
NG-$CoTe_2$/CRF	2 M KOH	301 F g^{-1} @ 1 Ag^{-1}	98.6 / 5000	[12]
$ZnFe_2O_4$-rGO	2 M KOH	352.9 F g^{-1}@1 A g^{-1}	92/10000	[13]
1T′-$MoTe_2$ nanosheets	2 M KOH	1393 F g^{-1} @1 A g^{-1}	87 (50 A g^{-1})/ 1000	[14]
CoTe NRs	3.5 M KOH	170 C·g^{-1} @ 0.5 A·g^{-1}	99 / 5000	[15]

Table S3. Two-electrode supercapacitor devices using the various TMDs electrodes.

Electrode materials	Specific capacitance	Energy density	Power density	Capacitance retention (%)/cycles	Ref.
MCT-3//AC	***271 F g^{-1} @ 1 A g^{-1}***	***122 W h kg^{-1}***	***2000 W kg^{-1}***	***90 / 10000***	***This work***
CoTe//AC	192.1 $F \cdot g^{-1}$ @ 1 $A \cdot g^{-1}$	67 Wh Kg^{-1}	793 W kg^{-1}	94.8 / 5000	1
NiTe//AC	94.6 F g^{-1}	33.6 Wh. kg^{-1}	807.1 W. kg^{-1}	81/3000	2
NiTe/ZIF-67//AC	62.6 $F \cdot g^{-1}$ @ 0.2 $A \cdot g^{-1}$	45.3 Wh Kg^{-1}	5689.1 W kg^{-1}	94.8 / 5000	3
$MoTe_2$/graphene - symmetric	138 $F \cdot g^{-1}$ @ 1 $A \cdot g^{-1}$	43.2 Wh kg^{-1}	3000 W kg^{-1}	98/10000	4
$MoTe_2$//AC	138 F g^{-1} @ 2 A g^{-1}	49 Wh kg^{-1}	961 W kg^{-1}	95.5 / 5000	5
Nf@CCT@NT//AC	274 $F \cdot g^{-1}$ @ 1 $A \cdot g^{-1}$	41.92 Wh kg^{-1}	33573.7 W kg^{-1}	89.35 / 10000	6
SS/MWCNTs/ $MoTe_2$ - symmetric	68.01 @ 0.2 $mA.cm^{-2}$	18.51 Wh kg^{-1}	416 W kg^{-1}	94 / 2000	7
CoTe/$NiCo_2S_4$//AC	88.89 F g^{-1} @ 1 A g^{-1}	39.8 Wh kg^{-1}	832 W kg^{-1}	86.61 / 8000	8
$NiCoTe_2$//caC@pC	143 $F \cdot g^{-1}$ @ 1 $A \cdot g^{-1}$	50.84 Wh Kg^{-1}	790.05W kg^{-1}	87.88 /25000	9
Co_2Te_2@rGO//AC	64 $mAh \cdot g^{-1}$ @ 1 $A \cdot g^{-1}$	51 Wh kg^{-1}	800 W kg^{-1}	82 / 3000	11
NG-$CoTe_2$/CRF//AC	140.2 F g^{-1} @ 1 A g^{-1}	49.8 Wh kg^{-1}	985 W kg^{-1}	125.2 / 5000	12
$Cu_{0.5}Co_{0.5}Se_2$// MXene	321 $F \cdot g^{-1}$ @ 1 $A \cdot g^{-1}$	84.19 Wh kg^{-1}	715.12 W kg^{-1}	91.1/10000	16
CoTe (4:1)//AC	169 $F \cdot g^{-1}$ @ 0.5 $A \cdot g^{-1}$	60 Wh kg^{-1}	798 W kg^{-1}	74 / 10000	17

CF@$CoTe_2$-$NiTe_2$//CF@Fe_2O_3	131 $F \cdot g^{-1}$ @ 1 $A \cdot g^{-1}$	41 Wh kg^{-1}	750 W kg^{-1}	87.6 / 5000	[18]
1Td WTe_2 Nanosheets - symmetric	221 F g^{-1}	31 Wh kg^{-1}	7.8 kW kg^{-1}	91 / 5500	[19]
NiTe:Co//AC	103.4 F g^{-1}@ 1 A g^{-1}	36.8 Wh kg^{-1}	-	95 / 52000	[20]
1T′-$MoTe_2$/AC	158.9 F g^{-1}@ 1A g^{-1}	56.4 Wh kg^{-1}	0.8 k W kg^{-1}	-	[21]
CoTe@C–NiF – symmetric	296.27 mF cm^{-2}	43.84 Wh kg^{-1}	738.88 W kg^{-1}	83.33 / 8000	[22]
CoOTe//AC	621 $F \cdot g^{-1}$ @ 1 $A \cdot g^{-1}$	72.82 Wh kg^{-1}	0.635 kW kg^{-1}	90.88/20000	[23]

References

1. B. Ye, C. Gong, M. Huang, Y. Tu, X. Zheng, L. Fan, J. Lin and J. Wu, *Improved performance of a CoTe//AC asymmetric supercapacitor using a redox additive aqueous electrolyte*, *RSC Advances*, 2018, **8**, 7997–8006.
2. P. Zhou, L. Fan, J. Wu, C. Gong, J. Zhang and Y. Tu, *Facile hydrothermal synthesis of NiTe and its application as positive electrode material for asymmetric supercapacitor*, *J. Alloys Compd.*, 2016, **685**, 384–390.
3. K. L. Meghanathan, M. Parthibavarman, V. Sharmila and J. R. Joshua, *Metal-organic framework-derived Nickle Tellurideporous structured composites electrode materials for asymmetric supercapacitor application*, *Journal of Energy Storage*, 2023, **72**, 108665.
4. S. Sarwar, Z. Liu, J. Li, Y. Wang, R. Wang and X. Zhang, *High performance hybrid-capacitor based on MoTe2/graphene through ultra-fast, facile microwave-initiated synthesis*, *Journal of Alloys and Compounds*, 2020, **846**, 155886.
5. D. Vikraman, S. Hussain, K. Karuppasamy, P. Santhoshkumar, A. Kathalingam, J. Jung and H.-S. Kim, *Fabrication of asymmetric supercapacitors using molybdenum dichalcogenide nanoarray structures*, *Int. J. Energy Res.*, 2022, **46**, 18410–18425.

6. H. Arabdashti, A. M. Zardkhoshoui, A. Sadeghi and S. S. H. Davarani, *Integration of CuTe-CoTe nanosheets with NiTe2 nanoflowers for hybrid supercapacitor*, *Journal of Alloys and Compounds*, 2025, **1011**, 178427.
7. S. S. Karade and B. R. Sankapal, *Materials Mutualism through EDLC-Behaved MWCNTs with Pseudocapacitive $MoTe_2$ Nanopebbles: Enhanced Supercapacitive Performance*, *ACS Sustainable Chem. Eng.*, 2018, **6**, 15072–15082.
8. S. Wu, J. Wang, L. Zhao, Y. Cao, H. Yang, X. Jing, J. Li, Y. Zhao, J. Gong and Y. Dai, *High-performance asymmetric supercapacitor applications enabled by nickel foam-supported CoTe/NiCo2S4 core-shell nanorods*, *Journal of Alloys and Compounds*, 2025, **1022**, 180023.
9. F. Yang, M. Yang, J. Zhang, H. Guo, T. Zhang, H. Guo and W. Yang, *High-efficiency hybrid supercapacitor based on three-dimensional interconnected nitrogen-rich caCTF-1 @pC-C3N4 network and NiCoTe2*, *Journal of Alloys and Compounds*, 2022, **911**, 164782.
10. H. Mao, J. Yu, J. Li, T. Zheng, J. Cen and Y. Ye, *A high-performance supercapacitor electrode based on nanoflower-shaped CoTe2*, *Ceramics International*, 2020, **46**, 6991–6994.
11. M. Farshadnia, A. A. Ensafi, K. Z. Mousaabadi, B. Rezaei and M. Demir, *Facile synthesis of NiTe2-Co2Te2@rGO nanocomposite for high-performance hybrid supercapacitor*, *Scientific Reports*, 2023, **13**, 1364.
12. W. Han, J. Li, H. Ju, L. Yuan, X. D. Liu and C. Wang, *Nitrogen-Doped Graphitic Carbon-CoTe2 Decorated on Carbon Aerogel Microspheres as a High-Rate and Ultra-Stable Electrode for Efficient Capacitive Storage*, *ChemistrySelect*, 2024, **9**, e202405427.
13. S. Yang, Z. Han, J. Sun, X. Yang, X. Hu, C. Li and B. Cao, *Controllable ZnFe2O4/reduced graphene oxide hybrid for high-performance supercapacitor electrode*, *Electrochimica Acta*, 2018, **268**, 20–26.
14. M. Liu, Z. Wang, J. Liu, G. Wei, J. Du, Y. Li, C. An and J. Zhang, *Synthesis of few-layer 1T'-MoTe2 ultrathin nanosheets for high-performance pseudocapacitors*, *Journal of Materials Chemistry A*, 2017, **5**, 1035–1042.

15. M. Manikandan, K. Subramani, M. Sathish and S. Dhanuskodi, *Hydrothermal synthesis of cobalt telluride nanorods for a high performance hybrid asymmetric supercapacitor*, *RSC Advances*, 2020, **10**, 13632–13641.
16. Y. A. Dakka, J. Balamurugan, R. Balaji, N. H. Kim and J. H. Lee, *Advanced Cu0. 5Co0. 5Se2 nanosheets and MXene electrodes for high-performance asymmetric supercapacitors*, *Chemical Engineering Journal*, 2020, **385**, 123455.
17. W. Younas, M. K. Tufail, G. Mao, L. Wang, P. He, J. Tang, Q. Liu and R. Wang, *Morphology evolution of the CoTe2 nanosheets from nanoparticles: Structure-performance relationship to unlock high-energy-density supercapacitors*, *Journal of Power Sources*, 2025, **657**, 238189.
18. C. Shi, Q. Yang, S. Chen, Y. Xue, Y. Hao and Y. Yan, *Granular Nanosheets Made of Interconnected NiTe2-CoTe2 Nanoparticles on Carbon Fibers for High-Performance Hybrid Supercapacitors*, *ACS Applied Energy Materials*, 2022, **5**, 2817–2825.
19. P. Yu, W. Fu, Q. Zeng, J. Lin, C. Yan, Z. Lai, B. Tang, K. Suenaga, H. Zhang and Z. Liu, *Controllable Synthesis of Atomically Thin Type-II Weyl Semimetal WTe2 Nanosheets: An Advanced Electrode Material for All-Solid-State Flexible Supercapacitors*, *Advanced Materials*, 2017, **29**, 1701909.
20. B. Ye, M. Huang, L. Fan, J. Lin and J. Wu, *Co ions doped NiTe electrode material for asymmetric supercapacitor application*, *Journal of Alloys and Compounds*, 2019, **776**, 993–1001.
21. M. Liu, Z. Wang, J. Liu, G. Wei, J. Du, Y. Li, C. An and J. Zhang, *Synthesis of few-layer 1T'-MoTe 2 ultrathin nanosheets for high-performance pseudocapacitors*, *Journal of Materials Chemistry A*, 2017, **5**, 1035–1042.
22. T. Kshetri, T. I. Singh, Y. S. Lee, D. D. Khumujam, N. H. Kim and J. H. Lee, *Metal organic framework-derived cobalt telluride-carbon porous structured composites for high-performance supercapacitor*, *Composites Part B: Engineering*, 2021, **211**, 108624.
23. Y. Li, K. Donatien-Pascal and X. Jin, *In situ growth of Chrysanthemum-like NiCo2S4 on MXene for High-performance Supercapacitors and Non-enzymatic H2O2 Sensor*, *Dalton Transactions*, 2020.